

# Rotating and non-linear magnetic-charged black hole surrounded by quintessence

Carlos A. Benavides-Gallego,<sup>1,\*</sup> A. A. Abdujabbarov,<sup>1,2,†</sup> and Cosimo Bambi<sup>1,‡</sup>

<sup>1</sup>Center for Field Theory and Particle Physics and Department of Physics, Fudan University, 200438 Shanghai, China

<sup>2</sup>Ulugh Beg Astronomical Institute, Astronomicheskaya 33, Tashkent 100052, Uzbekistan

(Dated: June 23, 2022)

In this work we derived a rotating and non-linear magnetic-charged black hole surrounded by quintessence using the Newman-Janis algorithm. Considering the state parameter  $\omega_q = -3/2$ , we studied the event horizons, the ergosphere, and the ZAMO. We found that the existence of the outer horizon is constrained by the values of the charge  $Q$ . Furthermore, we found that the ergoregion increases when both the charge  $Q$  and the spin parameter  $a$  are increased. On the other hand, regarding equatorial circular orbits, we studied the limit given by the static radius on the existence of circular geodesics, the photon circular geodesics, and the innermost stable circular orbits (ISCO). We show that photon circular orbits do not depend strongly on  $Q$ , and  $r_{ISCO}$  is constrained by the values of charge.

## I. INTRODUCTION

Nowadays, the Standard Model of Cosmology (SMC) is the best theory available for the description of the Universe. It is based on two fundamental ingredients: the standard model of particle physics, and the general theory of relativity [1]. The success of the SMC lies on the fact that it agrees with three observational pillars in cosmology: the Hubble's law, the primordial abundances of light elements (Big Bang nucleosynthesis), and the cosmic microwave background: “the black body radiation left over from the first few hundred thousand years” [2]. Nevertheless, the SMC faces some problems if it is based only on these two fundamental ingredients [1]:

- (i) According to the small angular anisotropies detected in the CMB [3], different parts of the sky were causally connected at the time of the last scattering. Nevertheless, this is not what one would expect from the Friedmann equations if we consider a universe dominated by matter or radiation. This is known as the horizon problem.
- (ii) In the case of usual matter, Friedmann equations show that a strong departure from flatness is developed by time. Nevertheless, observations indicate that the universe is close to the geometrically flat case. As a result, the universe must be extremely fine-tuned to a flat one at the very beginning creating the so-called flatness problem.
- (iii) A mechanism to generate primordial inhomogeneities at cosmological scales is needed. These inhomogeneities are the seeds of future galaxies.
- (iv) Finally, beyond the framework of the standard model of particle physics, the formation of dangerous relics are expected at early times. These relics,

in the form of heavy particles or topological defects, would force the universe to recollapse too soon.

Inflation is one way to solve the problems of the horizon, flatness and dangerous relics. This idea was suggested by Kazanas and Starobinsky (1979), and Guth (1981) [4–7]. In this scenario, if the universe is supercooled to temperatures below the critical temperature for some phase transition in its early history, then a huge expansion factor would result from a period of exponential growth. This paradigm, according to Guth, is completely natural in the context of grand unified models of elementary particle interactions [6]. However, since the concrete mechanism of inflation suggested by Guth was not realistic, it became necessary to suggest a new inflationary model. In this sense, by introducing a dynamical inflation field, responsible for the exponential expansion of the universe, Linde and, independently, Albrecht and Steinhardt were able to solve this problem [8, 9]. Now many different scenarios of inflation are worked out and there is common agreement that a sufficiently long period of inflation could solve all the four problems mentioned above [1].

On the other hand, observations suggest that only 5% of the Universe is made of protons and neutrons, while 25% seems to be made of some weakly interactive particles known as dark matter. The remaining 70% seems to be a uniformly distributed hypothetical fluid with an unusual equation of state  $p \approx -\rho$  (where  $p$  is the pressure and  $\rho$  is the energy density). Scientists believe, based on the observation of the luminosity distances of type-I supernovae [10, 11] that the current acceleration is an effect of this hypothetical fluid [12]. This substance is known as dark energy and recent models suggest two possibilities for it: the cosmological constant [13–16], and the quintessence [17–22].

The quintessence is a scalar field with the state parameter  $\omega_q$  in the range  $-1 \leq \omega_q \leq -1/3$ , where the case  $\omega_q = -1$  covers the cosmological constant term [23]. In the case of black holes, for example, the

\* abgcarlos17@fudan.edu.cn

† ahmadjon@fudan.edu.cn

‡ Corresponding author: bambi@fudan.edu.cn

quintessence perturbs the black hole background metric and also modifies the curves of space-time around the singularity. Moreover, cosmological horizons exist in the space-time of black holes or other compact objects immersed in this kind of scalar field. The quintessence scenario can be realized in large variety of models: scalar field in modified  $f(R)$  gravity, string-like cosmology, k-essence, extra dimensions, braneworld models [24].

Interesting work considering the quintessence scenario has been done. In reference [23], for example, the general solutions to the spherically symmetric Einstein equations describing the Schwarzschild black hole surrounded by dark energy, in the form of a quintessential field, was found by Kiselev. Using this approach he was able to explain the asymptotic behaviour of the rotation curves in spiral galaxies. Furthermore, in reference [25], the same author presents a new static spherically symmetric exact solutions of the Einstein field equations for quintessential matter surrounding a black hole (charged or uncharged) and discusses the case in which  $w_q = -2/3$ .

On the other hand, and motivated by the importance of the geodesic structure in a space-time surrounded by quintessence, a detailed study of the photon trajectories was done in reference [26]. In [26] the authors obtained an exact solution for the trajectories in terms of the Jacobi elliptic integrals. A study of the motion and collision of particles in the gravitational field of rotating black hole immersed in quintessential dark energy was done in reference [27]. The authors of Ref. [27] focus on the acceleration of particles due to collisional processes and show how the centre of mass energy depends on the quintessential field parameter  $C$ . They also study the dependence of the maximal value of the efficiency of energy extraction through the Penrose process for rotating black holes with quintessential field parameter  $C$ . The authors found that the quintessence field decreases the energy extraction efficiency through the Penrose process and when the parameter  $C$  vanish it is possible to obtain the standard value of the efficiency coefficient for the Kerr black hole.

In reference [28], the shadow of a rotating black hole with quintessential energy was studied in vacuum, and in the presence of plasma. In [28] the authors found that, in the vacuum case, the quintessential parameter changes the shape of the shadow considerably. On the other hand, in the case of a quintessence black hole surrounded by plasma, the shape of the shadow depends on the plasma parameters, black hole spin, and the quintessential field parameter. However, for larger values of the quintessential field parameter, the shape of the shadow does not change significantly.

In this paper, we study a rotating and non-linear magnetic-charged black hole surrounded by quintessence.

The manuscript is organized as follow. In section II, we review the geometry of quintessential rotating black holes discussed in reference [24]. Then, in section III, we obtain the rotating solution of a non-linear magnetic-charger black hole surrounded by quintessence. In section IV, we consider the case  $w_q = -2/3$  and study the event horizon, the ergosphere, and the angular velocity of a zero angular momentum observer (ZAMO). Finally, in section V, we study the equatorial circular orbits, the static radius, the photon circular orbits, and the innermost stable circular orbits (ISCO).

Along the manuscript geometrized units ( $G = 1$  and  $c = 1$ ) and the signature  $(-+++)$  were used. Moreover, we set the mass of the black hole  $M = 1$  for all the figures and calculations.

## II. QUINTESSENTIAL ROTATING BLACK HOLE SOLUTIONS

The Newman-Janis algorithm (NJA) is used to obtain rotating space-times from a spherically symmetric background without solving Einstein's field equations. This mathematical idea was first proposed by E. T. Newman and A. I. Janis in 1965 [29]. Using this “*curious derivation*”, they were able to obtain Kerr's metric by performing a complex coordinate transformation on the Schwarzschild line element [29]. The key point behind the NJA lies on the fact that the contravariant tensor  $g^{\mu\nu}$ , expressed in Eddington-Finkelstein (EF) coordinates, can be defined in terms of a null tetrad.

The NJA has been widely used in the scientific community (see, e.g. [30–36] and references therein). Nevertheless, in order to obtain the general equations to find quintessential rotating black hole solutions, the authors of Ref. [24] used a modified version. As the authors explain, the only difference from the original NJA is that they skipped the complexification of coordinates [37–40].

In this section, we review the modified algorithm used in [24] to obtain the rotating solution of a black hole with quintessence energy. This algorithm can be divided into three important steps. First, it is important to transform the spherically symmetric line element from the Boyer-Lindquist (BL) to Eddington-Finkelstein (EF) coordinates. Then, since the contravariant components of the metric tensor can be expressed by a null tetrad, the next step is to perform a complex coordinate transformation. This transformation enables us to obtain the form of the contravariant tensor  $g^{\mu\nu}$  in terms of the tetrad. Finally, once the contravariant components of the metric are obtained, we turn back from EF to BL coordinates. This transformation involves two functions of  $r$ :  $\lambda(r)$  and  $\chi(r)$ . These functions can be found under the condition that all non-diagonal components of the

metric, with the exception of  $g_{t\phi}$ , vanish.

A spherically symmetric space-time, expressed in Boyer-Lindquist (BL) coordinates  $(t, r, \theta, \phi)$ , can be described by the line element [24]

$$ds^2 = -f(r)dt^2 + g^{-1}(r)dr^2 + h(r)d\Omega^2, \quad (1)$$

where

$$d\Omega^2 = d\theta^2 + \sin^2 \theta d\phi^2. \quad (2)$$

Hence, after using the coordinate transformation

$$du = dt - \frac{dr}{\sqrt{fg}}, \quad (3)$$

the line element in equation (1) takes the form

$$ds^2 = -f(r)du^2 - 2\sqrt{\frac{f(r)}{g(r)}}dudr + h(r)d\theta^2 + h(r)\sin^2 \theta d\phi^2. \quad (4)$$

The last expression is just the line element (1) expressed in EF coordinates  $(u, r, \theta, \phi)$ .

As mentioned above, the contravariant tensor  $g^{\mu\nu}$ , obtained from the line element in equation (4), can be expressed in terms of the null tetrad by the following relations [24]

$$g^{\mu\nu} = -l^\mu n^\nu - l^\nu n^\mu + m^\mu \bar{m}^\nu + m^\nu \bar{m}^\mu, \quad (5)$$

where

$$\begin{aligned} l^\mu &= \delta_r^\mu, \\ n^\mu &= \sqrt{\frac{g(r)}{f(r)}}\delta_\nu^\mu - \frac{f(r)}{2}\delta_\nu^\mu, \\ m^\mu &= \frac{1}{\sqrt{2h(r)}}\delta_\theta^\mu + \frac{i}{\sqrt{2h(r)}\sin\theta}\delta_\phi^\mu, \\ \bar{m}^\mu &= \frac{1}{\sqrt{2h(r)}}\delta_\theta^\mu - \frac{i}{\sqrt{2h(r)}\sin\theta}\delta_\phi^\mu. \end{aligned} \quad (6)$$

Note that the vectors  $l^\mu$  and  $n^\mu$  are real, while  $m^\mu$  is a complex vector. Furthermore, we use the notation in which  $\bar{m}^\mu$  is the complex conjugate of  $m^\mu$ . These vectors satisfy the orthogonality and isotropic conditions [24, 29]

$$l^\mu m_\mu = l^\mu \bar{m}_\mu = n^\mu m_\mu = n^\mu \bar{m}_\mu = 0, \quad (7)$$

and

$$l^\mu l_\mu = n^\nu n_\nu = m^\mu m_\nu = \bar{m}^\mu \bar{m}_\nu = 0, \quad (8)$$

respectively.

Now, from equation (5), it is possible to consider a complex transformation, not of the line element (4), but

of the tetrad in equation (6). Thus, after using the transformation [24]

$$u \rightarrow u - ia \cos \theta, \quad r \rightarrow r + ia \cos \theta, \quad (9)$$

the tetrad in equation (6) takes the form

$$\begin{aligned} l^\mu &= \delta_r^\mu, \\ n^\mu &= \sqrt{\frac{G}{F}}\delta_u^\mu - \frac{1}{2}F\delta_r^\mu, \\ m^\mu &= \frac{1}{\sqrt{2\Sigma}} \left[ \delta_\theta^\mu + ia(\delta_u^\mu - \delta_r^\mu) \sin \theta + \frac{i}{\sin \theta} \delta_\phi^\mu \right], \\ \bar{m}^\mu &= \frac{1}{\sqrt{2\Sigma}} \left[ \delta_\theta^\mu - ia(\delta_u^\mu - \delta_r^\mu) \sin \theta - \frac{i}{\sin \theta} \delta_\phi^\mu \right]. \end{aligned} \quad (10)$$

Here it is assumed that the functions  $f, g, h$  have changed to  $F, G$ , and  $\Sigma$  respectively (see [24] for details). Therefore, these functions depend on  $r, a$ , and  $\theta$ . Hence, with the help of equation (5), the contravariant components of the metric tensor in the new coordinate system are

$$\begin{aligned} g^{uu} &= \frac{a^2 \sin^2 \theta}{\Sigma}, \\ g^{ur} &= -\sqrt{\frac{G}{F}} - \frac{a^2 \sin^2 \theta}{\Sigma}, \\ g^{u\phi} &= \frac{a}{\Sigma}, \\ g^{rr} &= G + \frac{a^2 \sin^2 \theta}{\Sigma}, \\ g^{r\phi} &= -\frac{a}{\Sigma}, \\ g^{\theta\theta} &= \frac{1}{\Sigma}, \\ g^{\phi\phi} &= \frac{1}{\Sigma \sin^2 \theta}, \end{aligned} \quad (11)$$

and the covariant components of the metric tensor, which can be calculated using the relation

$$g^{\alpha\nu} g_{\alpha\mu} = \delta_\mu^\nu, \quad (12)$$

are

$$\begin{aligned} g_{uu} &= -F, \\ g_{ur} &= -\sqrt{\frac{F}{G}}, \\ g_{u\phi} &= a \left( F - \sqrt{\frac{F}{G}} \right) \sin^2 \theta, \\ g_{r\phi} &= a \sqrt{\frac{F}{G}} \sin^2 \theta, \\ g_{\theta\theta} &= \Sigma, \\ g_{\phi\phi} &= \sin^2 \theta \left[ \Sigma + a^2 \left( 2\sqrt{\frac{F}{G}} - F \right) \sin^2 \theta \right]. \end{aligned} \quad (13)$$

Then, we come back from the EF coordinates to BL coordinates by using the following transformations

$$\begin{aligned} du &= dt + \lambda(r)dr, \\ d\phi &= d\tilde{\phi} + \chi(r)dr. \end{aligned} \quad (14)$$

Where the functions  $\lambda(r)$  and  $\chi(r)$  can be found using the fact in which all non-diagonal components of the metric tensor, except the coefficient  $g_{t\phi}$  ( $g_{\phi t}$ ), are equal to zero. Therefore, we obtain that

$$\begin{aligned} \lambda(r) &= -\frac{k(r) + a^2}{g(r)h(r) + a^2}, \\ \chi(r) &= -\frac{a}{g(r)h(r) + a^2}, \end{aligned} \quad (15)$$

with

$$k(r) = \sqrt{\frac{g(r)}{f(r)}}h(r), \quad (16)$$

and

$$F(r, \theta) = \frac{(gh + a^2 \cos^2 \theta)\Sigma}{(k^2 + a^2 \cos^2 \theta)^2}, \quad (17)$$

$$G(r, \theta) = \frac{gh + a^2 \cos^2 \theta}{\Sigma}.$$

Finally, the rotating version of the spherically symmetric line element in equation (1) is

$$\begin{aligned} ds^2 &= -\frac{(gh + a^2 \cos^2 \theta)\Sigma}{(k + a^2 \cos^2 \theta)^2} dt^2 + \frac{\Sigma}{gh + a^2} dr^2 \\ &\quad - 2a \sin^2 \theta \left[ \frac{k - gh}{(k + a^2 \cos^2 \theta)^2} \right] \Sigma d\phi dt + \Sigma d\theta^2 \\ &\quad + \Sigma \sin^2 \theta \left[ 1 + a^2 \sin^2 \theta \frac{2k - gh + a^2 \cos^2 \theta}{(k + a^2 \cos^2 \theta)^2} \right] d\phi^2; \end{aligned} \quad (18)$$

where we have removed the tilde on  $\phi$ .

### III. ROTATING AND NON-LINEAR MAGNETIC CHARGED BLACK HOLE SOLUTION

The non-linear magnetic charged black hole surrounded by quintessence was obtained in reference [41] by considering Einstein gravity coupled to a non-linear electromagnetic field. It is described by the following equations

$$G_{\mu}^{\nu} = 2 \left[ \frac{\partial \mathcal{L}(F)}{\partial F} F_{\mu\rho} F^{\mu\rho} - \delta_{\mu}^{\nu} \mathcal{L}(F) + T_{\mu}^{\nu}(\text{quintessence}) \right], \quad (19)$$

with

$$\begin{aligned} \nabla_{\mu} \left( \frac{\partial \mathcal{L}(F)}{\partial F} F^{\mu\nu} \right) &= 0, \\ \nabla_{\mu} {}^* F^{\nu\mu} &= 0. \end{aligned} \quad (20)$$

Where  $\mathcal{L}(F)$  is a function of the invariant  $F_{\mu\nu}F^{\mu\nu}/4 \equiv F$ , and  $F_{\mu\nu}$  is the electromagnetic tensor defined by

$$F_{\mu\nu} = \partial_{\mu} A_{\nu} - \partial_{\nu} A_{\mu}. \quad (21)$$

In order to obtain the solution, the author considered the energy density of the quintessence given by

$$T_t^t = T_r^r = \frac{3\omega_q C}{2r^{3(\omega_q+1)}}. \quad (22)$$

Here  $C$  is the positive normalization factor (from now on the quintessence parameter) and  $\omega_q$  is the quintessential state parameter; which is constrained to the interval

$$-1 < \omega_q < -\frac{1}{3}. \quad (23)$$

The solution, in BL coordinates, is given by the line element

$$ds^2 = -f(r)dt^2 + f(r)^{-1}dr^2 + r^2 d\theta^2 + r^2 \sin^2 \theta d\phi^2, \quad (24)$$

with

$$f(r) = 1 - \frac{2Mr^2}{r^3 + Q^3} - \frac{C}{r^{3\omega_q+1}}. \quad (25)$$

Note that for  $C = 0$  the line element (24) reduces to the Hayward-Like black hole [42]; for  $Q = 0$  the metric reduces to the Schwarzschild solution surrounded by quintessence [25]. For  $C = 0$ ,  $Q = 0$  it reduces to the Schwarzschild black hole.

The rotating solution is obtained by using Eq. (18). In our case, we have that

$$\begin{aligned} g(r) = f(r) &= 1 - \frac{2Mr^2}{r^3 + Q^3} - \frac{C}{r^{3\omega_q+1}}, \\ h(r) = k(r) &= r^2. \end{aligned} \quad (26)$$

Thus, the line element (18) takes the form

$$\begin{aligned} ds^2 &= - \left[ 1 - \frac{2\rho r}{\Sigma} \right] dt^2 + \frac{\Sigma}{\Delta} dr^2 - \frac{4a\rho r \sin^2 \theta}{\Sigma} dt d\phi \\ &\quad + \Sigma d\theta^2 + \sin^2 \theta \left[ r^2 + a^2 + \frac{2a^2 \rho r \sin^2 \theta}{\Sigma} \right] d\phi^2, \end{aligned} \quad (27)$$

where

$$\begin{aligned} \Delta &= r^2 - 2\rho r + a^2, \\ \Sigma &= r^2 + a^2 \cos^2 \theta, \\ 2\rho &= \frac{2Mr^3}{Q^3 + r^3} + Cr^{-3\omega_q}. \end{aligned} \quad (28)$$

Q	C = 0.01			C = 0.02			C = 0.03			C = 0.04		
	r <sub>-</sub>	r <sub>+</sub>	r <sub>q</sub>	r <sub>-</sub>	r <sub>+</sub>	r <sub>q</sub>	r <sub>-</sub>	r <sub>+</sub>	r <sub>q</sub>	r <sub>-</sub>	r <sub>+</sub>	r <sub>q</sub>
0.100	0.080	2.034	97.95842168	0.080	2.079	47.91310621	0.080	2.129	31.196697	0.080	2.184	22.808295
0.205	0.159	2.0259	97.95842168	0.159	2.071	47.91310635	0.159	2.121	31.196698	0.159	2.176	22.808297
0.3	0.234	2.013	97.95842172	0.325	2.038	47.91310673	0.234	2.108	31.196699	0.234	2.163	22.808301
0.4	0.325	1.992	97.95842180	0.399	2.017	47.91310746	0.324	2.088	31.196702	0.316	2.145	22.808308
0.49	0.399	1.971	97.95842195	0.501	1.982	47.91310867	0.398	2.067	31.196706	0.393	2.124	22.808321
0.605	0.502	1.935	97.95842214	0.596	1.944	47.91311048	0.499	2.033	31.196713	0.498	2.090	22.808339
0.7	0.598	1.895	97.95842242	0.717	1.886	47.91311300	0.593	1.996	31.19672341	0.591	2.054	22.808365
0.81	0.722	1.836	97.95842279	0.717	1.886	47.91311635	0.713	1.941	31.196736	0.708	2.001	22.808400
0.9	0.839	1.770	97.95842328	0.830	1.825	47.91312065	0.823	1.884	31.196752	0.815	1.947	22.808444
1	1	1.666	97.95842384	0.982	1.730	47.91312573	0.966	1.797	31.1967730	0.951	1.868	22.808500

TABLE I. Values for the inner ( $r_-$ ), outer ( $r_+$ ), and quintessential ( $r_q$ ) horizons as a function of  $Q$  for different values of  $C$ . We set  $a = 0.1$  and  $M = 1$ .

#### IV. ROTATING BLACK HOLE WITH THE PARAMETER $\omega_q = -2/3$

In this section, we focus our attention to the case in which  $\omega_q = -2/3$ . Hence, after substitution, the line element in equation (27) reduces to

$$\begin{aligned}
ds^2 = & - \left(1 - \frac{2\rho r}{\Sigma}\right) dt^2 + \frac{\Sigma}{\Delta} dr^2 \\
& - \frac{4a\rho r \sin^2 \theta}{\Sigma} d\phi dt + \Sigma d\theta^2 \\
& + \sin^2 \theta \left( r^2 + a^2 + \frac{2\rho r a^2 \sin^2 \theta}{\Sigma} \right) d\phi^2,
\end{aligned} \tag{29}$$

where

$$\begin{aligned}
\Delta &= r^2 - 2\rho r + a^2, \\
\Sigma &= r^2 + a^2 \cos^2 \theta, \\
2\rho &= \frac{2Mr^3}{r^3 + Q^3} + Cr^2.
\end{aligned} \tag{30}$$

For  $Q = 0$  the metric reduces to the Kerr solution surrounded by quintessence [24]. When  $a = 0$ , we obtain the non-linear charged magnetic black hole obtained in reference [41]. Finally, for  $C = 0$ ,  $Q = 0$  and  $a = 0$  Eq. (27) reduces to the Schwarzschild black hole.

Now, we study the behaviour of the event horizon, the ergosphere, and the ZAMO.

##### A. Event horizons

To compute the event horizons we use the condition  $g^{rr} = 0$ . Therefore, for the line element (27), we obtain

$$g^{rr} = \frac{\Delta}{\Sigma} = \frac{a^2 - Cr^3 - \frac{2Mr^4}{Q^3 + r^3} + r^2}{a^2 \cos^2(\theta) + r^2}, \tag{31}$$

from which

$$\Delta = a^2 - Cr^3 - \frac{2Mr^4}{Q^3 + r^3} + r^2 = 0. \tag{32}$$

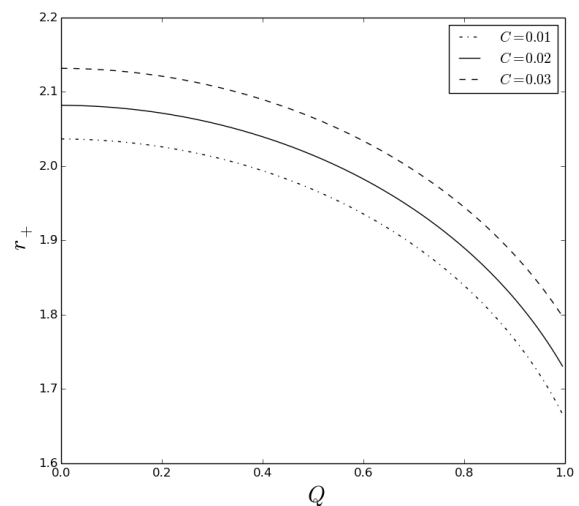


FIG. 1.  $r_+$  vs.  $Q$  for different values of  $C$ . We set  $a = 0.1$

Hence, equation (32) can be expressed as

$$Cr^6 - r^5 + 2r^4 - (a^2 - CQ^3)r^3 - Q^3r^2 - a^2Q^3 = 0. \tag{33}$$

This equation cannot be solved analytically but numerically. Therefore, in order to find the roots of equation (33), we set  $a = 0.1$  and considered different values of the quintessential parameter  $C$ . Then, for different values of  $Q$  in the interval  $0 \leq Q \leq 1$ , we compute the roots. We found three real roots:  $r_-$ ,  $r_+$  and  $r_q$ , which represent the inner and outer black hole horizons, and the quintessential cosmological horizon respectively.

Table I shows the values of the inner, outer, and quintessential horizon for different values of  $Q$  and  $C$ . From the Table I, we see that  $r_-$  and  $r_q$  increase while  $r_+$  decreases as  $Q$  increases. On the other hand, for fixed values of  $Q$ , the quintessential horizon  $r_q$  decrease while  $r_+$  increase as  $C$  increases.

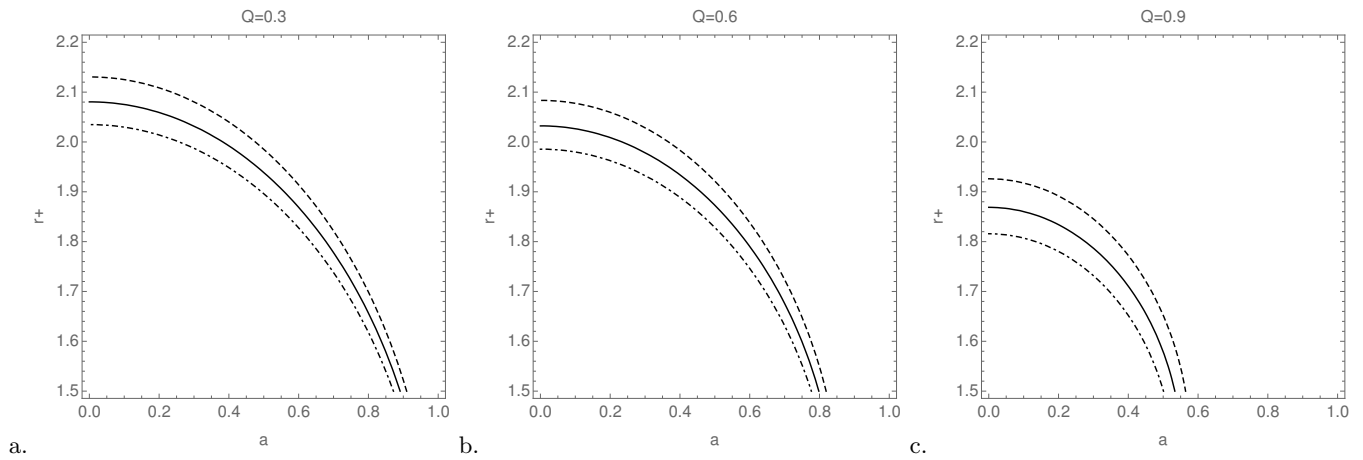


FIG. 2. Plot of the outer horizon  $r_+$  vs. the spin parameter  $a$  for different values of  $Q$  and  $C = 0.01$  (dot-dashedline),  $C = 0.02$  (continuous line), and  $C = 0.03$  (dashed line).

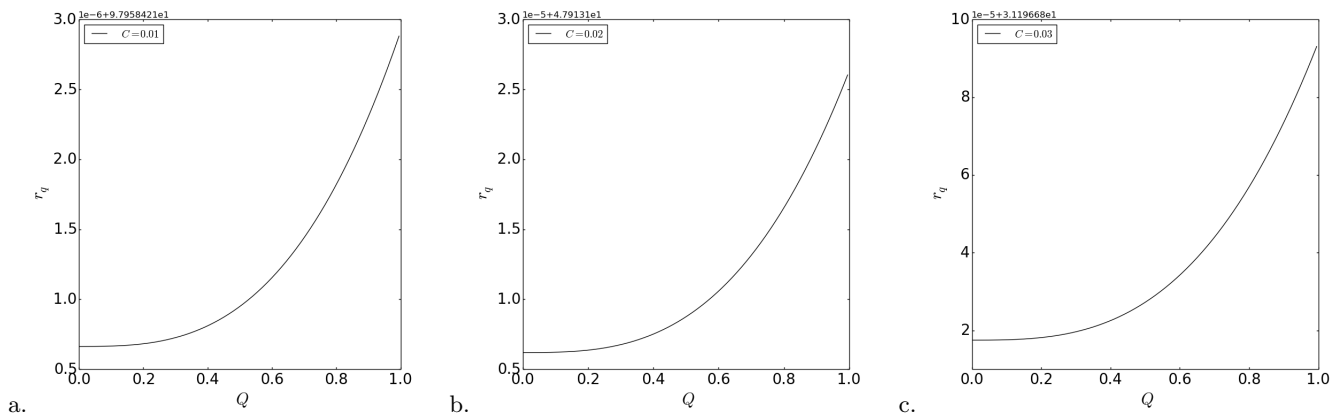


FIG. 3.  $r_q$  vs.  $Q$  for different values of  $C$ . Please note the scale used at the top of each plot. In figure *a*, for example, to the value 2.0 in the vertical axis corresponds to  $r_q = 97.95841 + 2 \times 10^{-6}$ . Similarly for figures *b* and *c*. We set  $a = 0.1$  in all the plots.

Fig. 1 shows the outer horizon  $r_+$  as a function of  $Q$ . In contrast with the inner horizon, the outer horizon  $r_+$  decreases when the charge  $Q$  increases. Furthermore, the bigger the values of  $C$ , the bigger the values of the outer radius. In Fig. 2, we plotted the outer radius  $r_+$  as a function of the spin parameter  $a$  for different values of  $Q$  and  $C$ . The values of  $r_+$  decreases as  $Q$  and  $a$  increases.

On the other hand, Fig. 3 shows the quintessential cosmological horizon as a function of the charge  $Q$  for different values of  $C$ . The behaviour is quite similar between figures:  $r_q$  increases as the charge  $Q$  increases. Note that the changes in the quintessential horizon are of order  $10^{-6}$  ( $C = 0.01$ ) and  $10^{-5}$  ( $C = 0.02$  and  $C = 0.03$ ) (see Table I for details). The value of  $r_q$  is bigger for small values of  $C$ . For example, for  $C = 0.01$  the value of the quintessential radius is of order  $r_q = 97.9584$  while for  $C = 0.03$  the value is

$r_q = 31.1966$ . As can be seen clearly from Fig. 3 *a* and *c*.

## B. Ergosphere

The ergosphere is a region located between the event horizon and the static limit surface, which is defined by the equation [24]

$$g_{tt}(r_{st}, \theta) = \left(1 - \frac{2\rho r_{st}}{\Sigma}\right) = 0. \quad (34)$$

Using the second and third equations in (30), we obtain

$$Cr_{st}^6 - r_{st}^5 + 2r_{st}^4 - (a \cos^2 \theta - CQ^3)r_{st}^3 - a^2Q^3 \cos^2 \theta = 0. \quad (35)$$

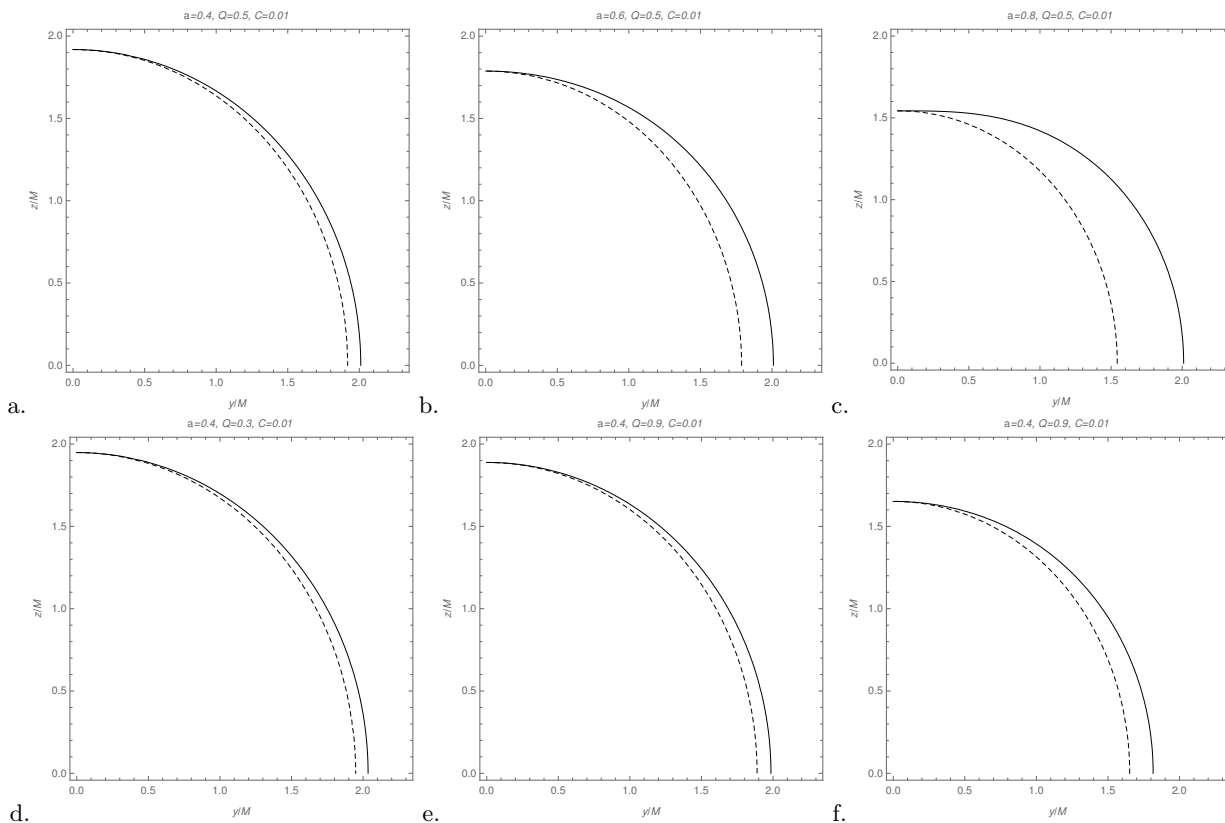


FIG. 4. Shape and size of the horizon (dashed line) and the ergosphere (continuous line) of the rotating and non-linear charged black hole.

In the equatorial plane ( $\theta = \pi/2$ ), equation (35) takes the form

$$Cr_{st}^6 - r_{st}^5 + 2r_{st}^4 + CQ^3r_{st}^3 = 0. \quad (36)$$

Note that, as in the case of Kerr black hole, at the equatorial plane  $r_{st}$  does not depend on the rotation parameter  $a$  (see Fig. 4 a, b and c). After factorization, equation (36) can be reduced to

$$Cr_{st}^3 - r_{st}^2 + 2r_{st} + CQ^3 = 0. \quad (37)$$

In the polar caps ( $\theta = 0, \pi$ ), equation (35) reduces to

$$Cr_{st}^6 - r_{st}^5 + 2r_{st}^4 - (a - CQ^3)r_{st}^3 - Q^3r_{st}^2 - a^2Q^3 = 0. \quad (38)$$

Note that the equations governing the event horizon and the ergosphere, equations (33) and (38) respectively, coincide at the polar caps. In agreement with the result obtained in [24].

In Fig. 4 we plot the shape and size of the horizon and the ergosphere. When the spin parameter  $a$  is increased, while keeping constant the charge  $Q$  and the quintessence parameter  $C$ , the radius of the event horizon decreases and the area of the ergo-region increases. Similar behaviour is observed when the charge  $Q$  is increased while keeping constant the spin and quintessence parameters.

Nevertheless, the increment of the ergo-region is stronger in the first case: when the spin parameter  $a$  is increased. On the other hand, from Figs. 4 d, e and f, we conclude that the ergosphere radius does depend on the charge  $Q$  in the equatorial plane.

### C. ZAMO

The geodesic motion of a particle on a space-time with metric  $g_{\mu\nu}$  is governed by the Lagrangian [43]

$$\mathcal{L} = \frac{1}{2}g_{\mu\nu}\dot{x}^\mu\dot{x}^\nu, \quad (39)$$

where the dot denotes the total derivative with respect to an affine parameter.

In equation (27), the components of the metric does not depend on the coordinates  $t$  and  $\phi$ . Therefore, two constants of motion are obtained: the specific energy  $E$ , and the axial component of the specific angular momentum  $L_z$ . Hence, after using the Euler-Lagrange equa-

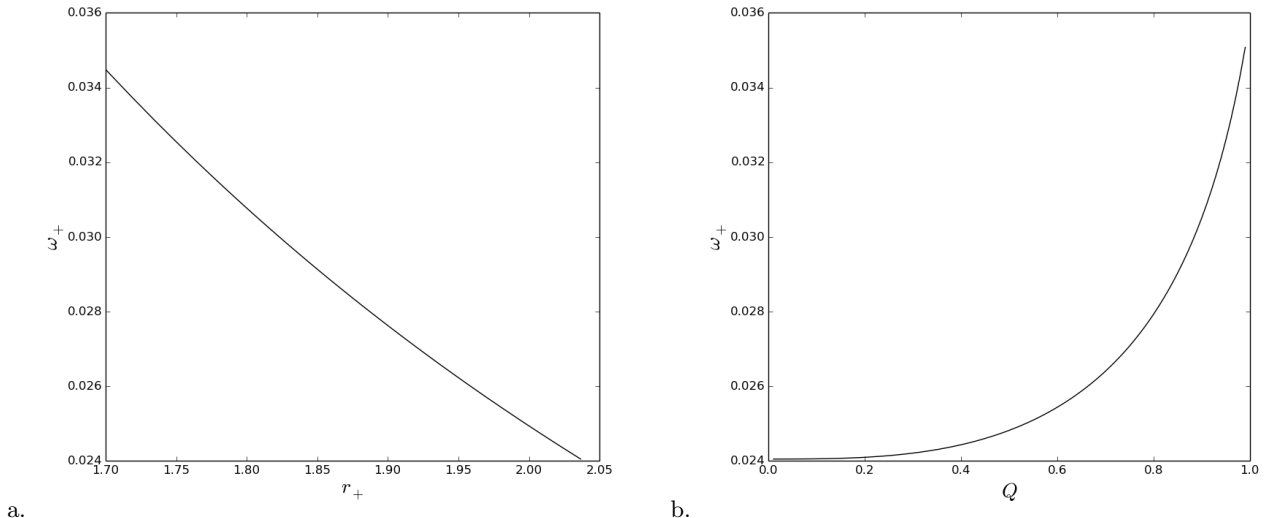


FIG. 5. **left panel:**  $\omega_+$  vs.  $Q$ . **Right panel:**  $\omega_+$  vs.  $r_+$ . In both plots we solve equation (33) setting  $a = 0.1$ , and  $C = 0.01$

tions, we obtain that [43]

$$\begin{aligned} \frac{\partial \mathcal{L}}{\partial \dot{t}} &= g_{tt} \dot{t} + g_{t\phi} \dot{\phi} = -E \\ \frac{\partial \mathcal{L}}{\partial \dot{\phi}} &= g_{t\phi} \dot{t} + g_{\phi\phi} \dot{\phi} = L_z \end{aligned} \quad (40)$$

In contrast with Newtonian gravity, where the angular momentum of a spinning object has no gravitational effect, in general relativity, the angular momentum alters the geometry of the space-time. In consequence, it is possible for a test-particle to have a non-vanishing angular velocity even if its specific angular momentum  $L_z$  vanishes [43]. This effect, known as dragging, can be obtained from the second equation in (40) after setting  $L_z = 0$ .

The angular velocity of a zero angular momentum observer (ZAMO) is defined by [44]

$$\omega = -\frac{g_{\phi t}}{g_{\phi\phi}}. \quad (41)$$

Thus, using the line element (27), we obtain that

$$\begin{aligned} \omega &= \frac{2a\rho r \sin^2 \theta}{\Sigma \sin^2 \theta \left( r^2 + a^2 + \frac{2\rho r a^2 \sin^2 \theta}{\Sigma} \right)} \\ &= \frac{2a\rho r}{(r^2 + a^2)^2 - a^2 \Delta \sin^2 \theta}. \end{aligned} \quad (42)$$

In the last step, we used the relation  $2\rho r = r^2 + a^2 - \Delta$  in the denominator. At the horizon  $r_h$ , where  $\Delta = 0$ , the ZAMO can be obtained by

$$\omega_h = \omega(r_h) = \frac{a}{r_h^2 + a^2}. \quad (43)$$

Note that  $r_h$  can be the inner, outer, or quintessential horizon.

In Fig. 5a and Fig. 5b it is plotted  $\omega_+$  as a function of  $Q$  and  $r_+$ , respectively. From the figures, we see that  $\omega_+ = \omega(r_+)$  increases as the charge increases, while it decreases as  $r_+$  increases. Note that the change in  $\omega_+$  is small in both cases.

## V. EQUATORIAL CIRCULAR ORBITS

In equation (39) we introduced the Lagrangian

$$\mathcal{L} = \frac{1}{2} g_{\mu\nu} \dot{x}^\mu \dot{x}^\nu. \quad (44)$$

Now, using the components of the metric tensor in equation (27) and considering the geodesic motion of a test particle in the equatorial plane ( $\theta = \pi/2$ ), the Lagrangian reduces to

$$2\mathcal{L} = g_{tt} \dot{t}^2 + g_{rr} \dot{r}^2 + 2g_{t\phi} \dot{t} \dot{\phi} + g_{\phi\phi} \dot{\phi}^2. \quad (45)$$

We have mentioned that the line element in equation (27) has two conserved quantities: the specific energy  $E$ , and the axial component of the specific angular momentum  $L_z$ . In this sense, the equations of motion are given by [27, 43]

$$\begin{aligned} p_t &= \frac{\partial \mathcal{L}}{\partial \dot{t}} = g_{tt} \dot{t} + g_{t\phi} \dot{\phi} = -E \\ p_\phi &= \frac{\partial \mathcal{L}}{\partial \dot{\phi}} = g_{t\phi} \dot{t} + g_{\phi\phi} \dot{\phi} = L_z \\ p_r &= \frac{\partial \mathcal{L}}{\partial \dot{r}} = g_{rr} \dot{r} \\ p_\theta &= \frac{\partial \mathcal{L}}{\partial \dot{\theta}} = 0. \end{aligned} \quad (46)$$

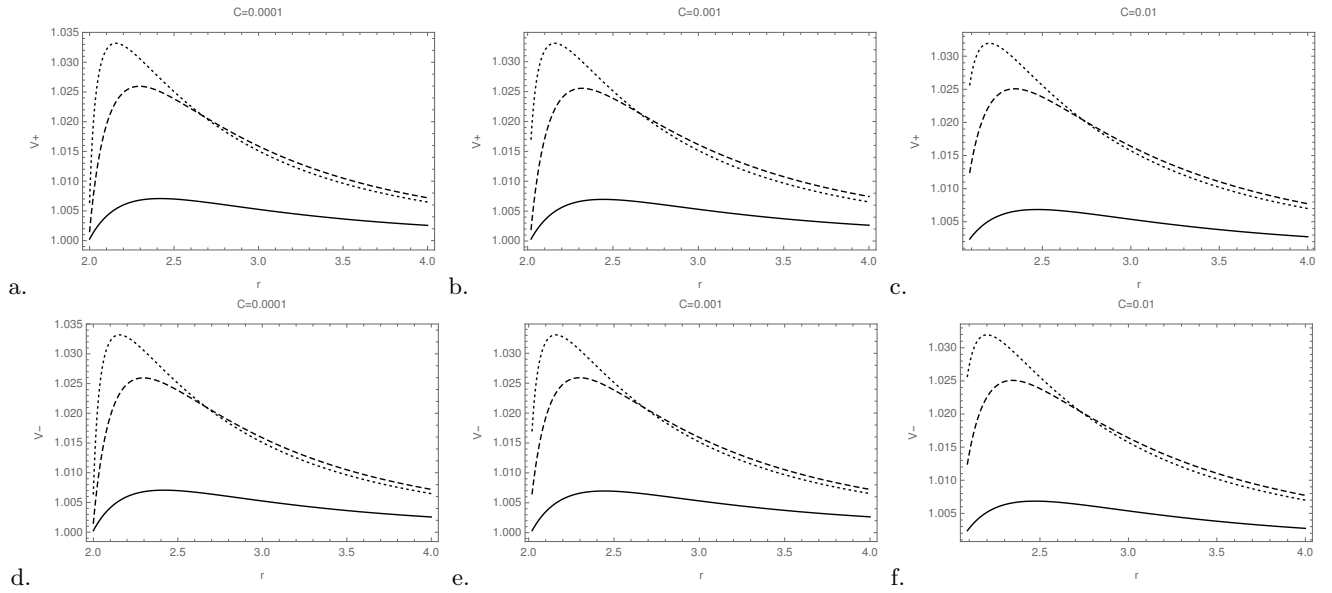


FIG. 6. Plot of  $V_+$  and  $V_-$  vs.  $r$  for different values of  $C$  when  $a = 0$  (dotted line),  $a = 0.3$  (Dot-Dashed line),  $a = 0.6$  (Dashed line), and  $a = 0.9$  (Continuous line). In all the figures we considered  $Q = 0.3$ ,  $\omega_q = -2/3$ .

On the other hand, the Hamiltonian

$$\mathcal{H} = \sum_i p_i \dot{x}_i - \mathcal{L}, \quad (47)$$

can be expressed in terms of the metric components as [27]

$$2\mathcal{H} = -E\dot{t} + g_{rr}\dot{r}^2 + L_z\dot{\phi} = \epsilon, \quad (48)$$

where  $\epsilon$  is equal to  $-1$ ,  $0$ , or  $1$  for time-like, light-like, and space-like geodesics, respectively.

Let's consider the first and second equations in (46). From the first equation, we have that

$$\dot{\phi} = -\frac{E + g_{tt}\dot{t}}{g_{t\phi}}, \quad (49)$$

then, replacing in the second equation of (46), we obtain

$$\dot{t} = \frac{g_{\phi\phi}E + L_z g_{t\phi}}{g_{t\phi}^2 - g_{\phi\phi}g_{tt}}, \quad (50)$$

from which, after substitution in equation (49), we obtain

$$\dot{\phi} = -\frac{g_{t\phi}E + g_{tt}L_z}{g_{t\phi}^2 - g_{\phi\phi}g_{tt}}. \quad (51)$$

Now, replacing equations (50) and (51) in equation (48) and considering particles moving along time-like geodesics ( $\epsilon = -1$ ), we obtain [43]

$$g_{rr}\dot{r}^2 = \frac{g_{\phi\phi}E^2 + 2g_{t\phi}EL_z + g_{tt}L_z^2}{g_{t\phi}^2 - g_{tt}g_{\phi\phi}} - 1. \quad (52)$$

According to equation (52), the effective potential is given by

$$V_{eff} = \frac{g_{\phi\phi}E^2 + 2g_{t\phi}EL_z + g_{tt}L_z^2}{g_{t\phi}^2 - g_{tt}g_{\phi\phi}}. \quad (53)$$

In the equatorial plane, circular orbits are located at the zeros and turning points of the effective potential. This means that  $\dot{r} = \dot{\theta} = 0$  from which  $V_{eff} = 0$ , and  $\ddot{r} = \ddot{\theta} = 0$  which requires that  $\partial_r V_{eff} = 0$  and  $\partial_\theta V_{eff} = 0$ , respectively. In this sense, we need to find the specific energy  $E$  and the axial component of the specific angular momentum  $L_z$ . In order to do so, we follow reference [43].

The geodesic equation

$$\frac{d^2 x^\mu}{d\tau^2} + \Gamma_{\alpha\beta}^\mu \frac{dx^\alpha}{d\tau} \frac{dx^\beta}{d\tau} = 0, \quad (54)$$

where  $\tau$  is an affine parameter, can be written in the form

$$\frac{d}{d\tau} (g_{\nu\alpha} \dot{x}^\alpha) = \frac{1}{2} (\partial_\nu g_{\alpha\beta}) \dot{x}^\alpha \dot{x}^\beta. \quad (55)$$

The radial component is given by the relation

$$\begin{aligned} \frac{d}{d\tau} (g_{rr}\dot{r}) &= \frac{1}{2} (\partial_r g_{tt} \dot{t}^2 + 2\partial_\phi g_{\phi t} \dot{\phi} \dot{t} + \partial_r g_{rr} \dot{r}^2 \\ &\quad + \partial_r g_{\theta\theta} \dot{\theta}^2 + \partial_r g_{\phi\phi} \dot{\phi}^2); \end{aligned} \quad (56)$$

since we are interested in equatorial circular orbits ( $\dot{r} = \dot{\theta} = \ddot{r} = 0$ ), the last expression reduces to

$$0 = \partial_r g_{tt} \dot{t}^2 + 2\partial_\phi g_{\phi t} \dot{\phi} \dot{t} + \partial_r g_{\phi\phi} \dot{\phi}^2. \quad (57)$$

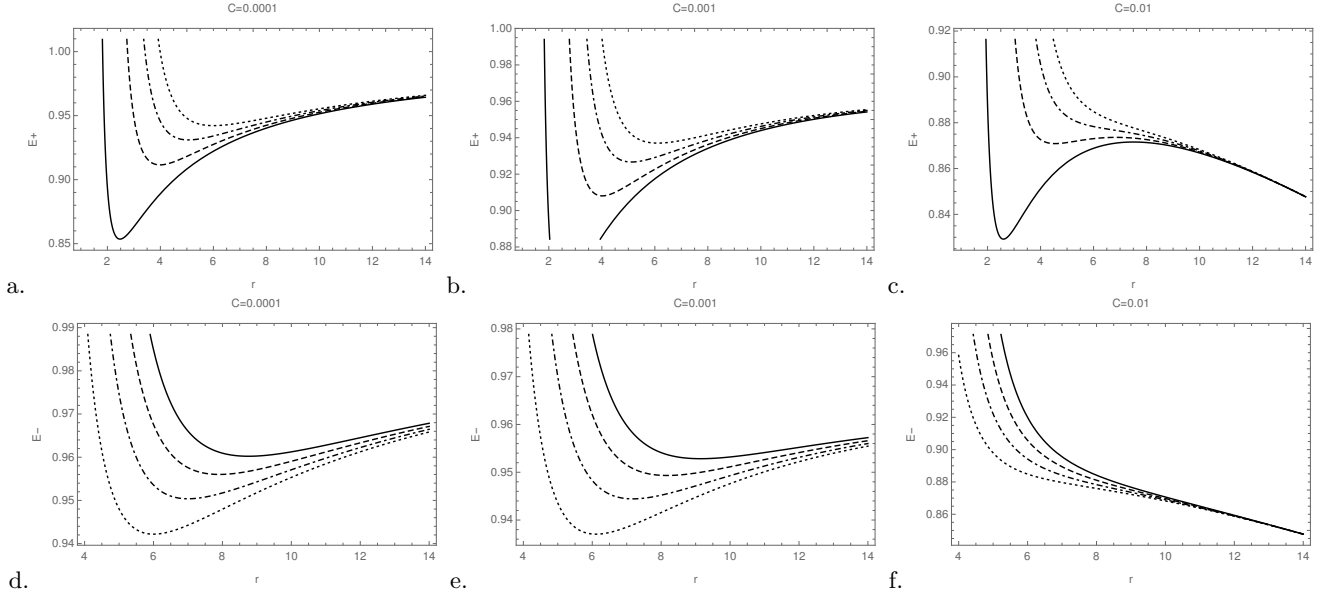


FIG. 7. Plot of  $E_+$  and  $E_-$  vs.  $r$  for different values of  $C$  when  $a = 0$  (dotted line),  $a = 0.3$  (Dot-Dashed line),  $a = 0.6$  (Dashed line), and  $a = 0.9$  (Continuous line). In all the figures we considered  $Q = 0.3$ ,  $\omega_q = -2/3$ .

Now, dividing by  $\dot{t}^2$  we obtain

$$0 = \partial_r g_{tt} + 2\partial_r g_{\phi t} \Omega + \partial_r g_{\phi\phi} \Omega^2, \quad (58)$$

where  $\Omega = \dot{\phi}/\dot{t}$  is the angular velocity. Equation (58) is a quadratic equation with solution

$$\Omega_{\pm} = \frac{-\partial_r g_{\phi t} \pm \sqrt{(\partial_r g_{\phi t})^2 - \partial_r g_{\phi\phi} \partial_r g_{tt}}}{\partial_r g_{\phi\phi}}. \quad (59)$$

According to equation (59), we have two possible orbits in the equatorial plane: co-rotating orbits ( $\Omega_+$ ), where the angular momentum is parallel to the spin of the central object; and the counter-rotating orbits ( $\Omega_-$ ), with the angular momentum anti-parallel to the spin of the central object.

The specific energy and angular momentum in equation (46) can be expressed as

$$\begin{aligned} (g_{tt} + g_{t\phi} \Omega) \dot{t} &= -E, \\ (g_{t\phi} + g_{\phi\phi} \Omega) \dot{t} &= L_z. \end{aligned} \quad (60)$$

Now, from  $g_{\mu\nu} \dot{x}^\mu \dot{x}^\nu = -1$  with  $\dot{r} = \dot{\theta} = 0$ , we have that

$$g_{tt} \dot{t}^2 + g_{t\phi} \dot{t} \dot{\phi} + g_{\phi\phi} \dot{\phi}^2 = -1, \quad (61)$$

from which, after using  $\Omega = \dot{\phi}/\dot{t}$ , we obtain that

$$\dot{t} = \frac{1}{\sqrt{-g_{tt} - 2g_{t\phi} \Omega - g_{\phi\phi} \Omega^2}}. \quad (62)$$

Therefore, in the equatorial plane, the specific energy and

angular momentum in equation (60) reduces to [43]

$$\begin{aligned} E &= -\frac{g_{tt} + g_{t\phi} \Omega_{\pm}}{\sqrt{-g_{tt} - 2g_{t\phi} \Omega_{\pm} - g_{\phi\phi} \Omega_{\pm}^2}}, \\ L_z &= \frac{g_{t\phi} + g_{\phi\phi} \Omega_{\pm}}{\sqrt{-g_{tt} - 2g_{t\phi} \Omega_{\pm} - g_{\phi\phi} \Omega_{\pm}^2}}. \end{aligned} \quad (63)$$

Where we use equation (59). Thus, after using the metric components, the specific energy and the angular momen-

tum reduces to [24]

$$\begin{aligned}
E_{\pm}^2 &= \frac{8\Delta(a^2 - \Delta)^2 + 2r\Delta\Delta'(a^2 - \Delta) - a^2r^2\Delta'^2}{r^2[16\Delta(\Delta - a^2) + r\Delta'(r\Delta' - 8\Delta)]} \\
&\pm \frac{2\sqrt{2}a\Delta\sqrt{(2a^2 - 2\Delta + r\Delta')^3}}{r^2[16\Delta(\Delta - a^2) + r\Delta'(r\Delta' - 8\Delta)]}, \\
L_{z\pm}^2 &= \frac{8a^2\Delta^3 - r^2(r^2 + a^2)^2\Delta'^2}{r^2[16\Delta(\Delta - a^2) + r\Delta'(r\Delta' - 8\Delta)]} \\
&- \frac{2\Delta^2[8a^2(r^2 + a^2) + 4r^4 + a^2r\Delta']}{r^2[16\Delta(\Delta - a^2) + r\Delta'(r\Delta' - 8\Delta)]} \\
&+ \frac{2(r^2 + a^2)\Delta[4a^2(r^2 + a^2) + r(3r^2 + a^2)\Delta']}{r^2[16\Delta(\Delta - a^2) + r\Delta'(r\Delta' - 8\Delta)]} \\
&\pm \frac{(r^2 + a^2)(2(r^2 + a^2) + r\Delta') - 2(2r^2 + a^2)\Delta}{r^2[16\Delta(\Delta - a^2) + r\Delta'(r\Delta' - 8\Delta)]} \\
&\times 2\sqrt{2}a\Delta\sqrt{(2a^2 - 2\Delta + r\Delta')^3}.
\end{aligned} \tag{64}$$

Here,  $(\prime)$  means the derivative with respect to  $r$ . The signs  $+$  and  $-$  stand for the co-rotating and counter-rotating particle orbits, respectively.

In Figs. 6-8 we plotted, respectively, the effective potential, and the specific energy and angular momentum of the co-rotating and counter-rotating circular orbits as a function of the radius for different values of the spin parameter  $a$  and the quintessence parameter  $C$ . From Fig. 7 co-rotating test particles (those with  $E_+$ ) are able to move along circular orbits that are closer to the black hole having small energy when the spin parameter is increased. The reason for such a behaviour lies in the fact that the radius of the event horizon decreases when the spin parameter of the black hole increases; as we have shown in Fig. 4.a, b, and c. On the other hand, counter-rotating particles are allowed to move far from the horizon with greater specific energy than the co-rotating particles.

### A. Static radius giving limit on the existence of circular geodesics

According to equation (64), the specific energy  $E_{\pm}$  will take real values if the condition [24]

$$2a^2 - 2\Delta - r\Delta' \geq 0 \tag{65}$$

is satisfied. Hence, equation (65) constrain the radius of the circular orbits to those values satisfying a relation

of the form  $r \leq r_C$ , where  $r_C$  is the *static radius* at which the test particle can be located at an unstable-equilibrium position. It was shown in [24] that at this point, the gravitational attraction of the black hole is just balanced by the cosmic repulsion due to the quintessential field.

In the case of the line element (27) the condition in equation (65) reduces to

$$Cr^6 - 2r^4 + 2CQ^3r^3 + 4Q^3r + CQ^6 \leq 0. \tag{66}$$

Note that equation (66) reduces to the condition

$$r \leq r_C \equiv \sqrt{\frac{2}{C}}, \tag{67}$$

when  $Q = 0$  (see equation (82) in reference [24]). Moreover, it is also important to point out that the condition in equation (66) is independent of  $a$ .

In Table II we show the static radius  $r_C$  for different values of  $C$  and  $Q$ . From the table, it is possible to see that, for constant values of the charge  $Q$ , the static radius decreases as the quintessence parameter  $C$  increases. On the other hand, for constant values of the quintessence parameter  $C$ , the static radius increases when the charge  $Q$  decreases but not significantly. For example, when  $C = 0.0005$  the value of  $r_C$  changes from 63.2456 to 63.2451, when the charge  $Q$  goes from 0.1 to 1, respectively.

### B. Photon circular geodesics

According to equation (63),  $E$  and  $L_z$  diverge when

$$g_{tt} + 2g_{t\phi}\Omega_{\pm} + g_{\phi\phi}\Omega_{\pm}^2 = 0. \tag{68}$$

It is known that this happens at the radius of the photon orbit  $r_{\gamma}$ . It is usual to find circular orbits for  $r > r_{\gamma}$  but not for  $r < r_{\gamma}$ . In such a case, the radius of the photon orbit is the equatorial circular orbit with the smallest radius for both massless and massive particles. In this sense, massive particles can reach the photon orbit in the limit of infinite specific energy  $E$ . However, in some particular space-times, such as quintessence space-time, circular orbits with  $r < r_{\gamma}$  may exist, and it is also possible the presence of two or more photon orbits [43].

From equation (64), we find that  $r_{\gamma}$  is given by the condition

$$16\Delta(\Delta - a^2) + r\Delta'(r\Delta' - 8\Delta) = 0, \tag{69}$$

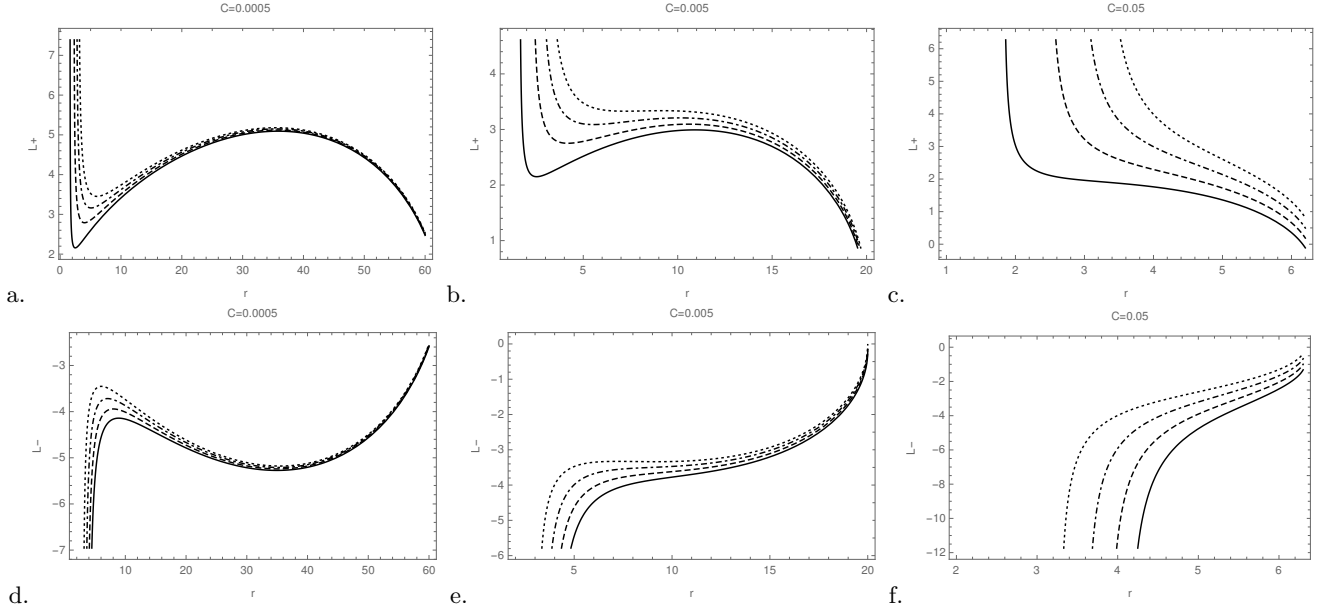


FIG. 8. Plot of  $L_+$  and  $L_-$  vs.  $r$  for different values of  $C$  when  $a = 0$  (dotted line),  $a = 0.3$  (Dot-Dashed line),  $a = 0.6$  (Dashed line), and  $a = 0.9$  (Continuous line). In all the figures we considered  $M = 1$ ,  $Q = 0.3$ ,  $\omega_q = -2/3$ .

Q	$C = 0.001$	$C = 0.002$	$C = 0.003$	$C = 0.01$	$C = 0.02$	$C = 0.03$
	$r_C$	$r_C$	$r_C$	$r_C$	$r_C$	$r_C$
0.1	44.7214	31.6228	25.8199	14.1421	9.99998	8.16494
0.2	44.7214	31.6228	25.8199	14.1421	9.99984	8.16473
0.3	44.7213	31.6227	25.8198	14.1419	9.99946	8.16416
0.4	44.7213	31.6226	25.8197	14.1415	9.99872	8.16304
0.5	44.72212	31.6225	25.8195	14.1409	9.9975	8.16121
0.6	44.7211	31.6223	25.8192	14.1387	9.99568	8.15847
0.7	44.7210	31.6221	25.8189	14.137	9.99313	8.15464
0.8	44.7208	31.6218	25.8184	14.1348	9.98973	8.14953
0.9	44.7206	31.6213	25.8177	14.1348	9.98536	8.14294
1	44.7204	31.6208	25.8169	14.1321	9.97989	8.13467

TABLE II. Values for the *static radius* ( $r_c$ ) for different values of  $Q$  and  $C$ . We set  $M = 1$ .

or

$$\begin{aligned}
0 = & 8a^2CQ^{12} + (32a^2Q^9 + 4Q^{12})r - 4CQ^{12}r^2 \\
& + (32a^2CQ^9 + C^2Q^{12})r^3 + (48a^2Q^6 + 16Q^9)r^4 \\
& - 16CQ^9r^5 + (48a^2CQ^6 - 24Q^6 + 4C^2Q^9)r^6 \\
& + (24Q^6 + 12CQ^6)r^7 - 24CQ^6r^8 \\
& + (32a^2CQ^3 - 48Q^3 + 6C^2Q^6)r^9 \\
& + (16Q^3 - 16a^2 + 24CQ^3)r^{10} \\
& + (36 - 16CQ^3)r^{11} + (8a^2C - 24 + 4C^2Q^3)r^{12} \\
& + (4 + 12C)r^{13} - 4Cr^{14} + C^2r^{15},
\end{aligned} \tag{70}$$

In order to study the behaviour of  $r_\gamma$ , we consider the case in which  $Q \ll 1$ . Therefore, equation (70) reduces to

$$C^2r^5 - 4Cr^4 + (4 + 12C)r^3 + (8a^2C - 24)r^2 + 36r - 16a^2 = 0. \tag{71}$$

In Table III we show the behaviour of  $r_\gamma$  for different values of the spin and quintessence parameters in the limit  $Q \ll 1$ . According to the table, when the spin  $a$  is constant and the quintessence parameter  $C$  increases, the photon radius  $r_{\gamma_2}$  increases while  $r_{\gamma_3}$  decreases. On the other hand, for fixed values of the quintessence parameter  $C$ ,  $r_{\gamma_2}$  decreases and  $r_{\gamma_3}$  increases when the spin parameter increases.

### C. Innermost Stable Circular Orbits (ISCO)

The radius of the innermost stable circular orbit (ISCO)  $r_{ISCO}$  is defined by [43]

$$\frac{\partial^2 V_{eff}}{\partial r^2} = 0. \tag{72}$$

Since the equatorial circular orbits at  $r < r_{ISCO}$  are unstable, in the Novikov-Thorne model for thin accretion

a	C = 0.001			C = 0.002			C = 0.003			C = 0.004		
	$r_{\gamma_1}$	$r_{\gamma_2}$	$r_{\gamma_3}$									
0.1	0.004457	2.886697	3.117851	0.004457	2.891229	3.122380	0.004457	2.895790	3.126936	0.004457	2.900380	3.131518
0.2	0.017992	2.763666	3.227286	0.017992	2.768169	3.231783	0.017992	2.772701	3.236306	0.017992	2.777262	3.240853
0.3	0.041119	2.634448	3.333277	0.041119	2.638900	3.337723	0.041119	2.643382	3.342191	0.041119	2.647893	3.346683
0.4	0.074793	2.497713	3.436197	0.074793	2.502093	3.440572	0.074792	2.506502	3.444968	0.074792	2.510942	3.449384
0.5	0.120613	2.351554	3.536355	0.120611	2.355841	3.540640	0.120609	2.360157	3.544943	0.120608	2.364503	3.549265
0.6	0.181230	2.193060	3.634010	0.181224	2.197235	3.638186	0.181218	2.201439	3.642378	0.181212	2.205671	3.646585
0.7	0.261301	2.017356	3.729381	0.261282	2.021405	3.733430	0.261263	2.025482	3.737491	0.261244	2.029587	3.741565
0.8	0.370088	1.814991	3.822657	0.370026	1.818922	3.826561	0.369964	1.822879	3.830473	0.369902	1.826863	3.834395
0.9	0.531638	1.561754	3.914002	0.531400	1.565677	3.917741	0.531162	1.569624	3.921487	0.530925	1.573595	3.925237
1	0.965119	1.038336	4.003565	0.951561	1.055371	4.007114	0.941481	1.068951	4.010674	0.933191	1.080763	4.014236

TABLE III. Values of  $r_{\gamma_1}$ ,  $r_{\gamma_2}$ , and  $r_{\gamma_3}$  for different values of  $a$  and  $C$ . We consider the limit  $Q \ll 1$ .

disks the inner edge of the disk is assumed at the ISCO radius [43].

In Fig. 9 we plot  $r_{ISCO}$  as a function of the spin parameter  $a$  for different values of  $Q$  when the quintessence parameter takes the values  $C = 0.001, 0.002$  and  $0.003$ . According to the figure,  $r_{ISCO}$  decreases as the spin  $a$  parameter increases. Note that the difference is bigger for small values of the spin parameter  $a$ . A similar effect is obtained when  $Q$  is increased. Moreover, the  $r_{ISCO}$  increases as the value of the quintessence parameter  $C$  increases. On the other hand, as Fig.9c shows, there are two regions (outside the event horizon  $r_+$ ) where the innermost stable circular orbits may exist. This feature, according to the figure, starts when the value of the spin parameter  $a = 0.589$  and ends at  $a = 0.671$  (approximately). For values of  $a$  greater than  $0.671$  the existence of  $r_{ISCO}$  is not possible.

## VI. CONCLUSION

In this work we have obtained the rotating solution of a non-linear magnetic-charged black hole surrounded by quintessence using a modified version of the NJA discussed in reference [24]. In section IV, using  $\omega_q = -2/3$ , we studied the behavior of the event horizon, the ergosphere, and the ZAMO for different values of the charge  $Q$ , the spin parameter  $a$  and the quintessence parameter  $C$ . In the case of the event horizons, we solved equation (33) numerically and found three solutions: the inner, outer, and quintessence horizons. According to the results shown in table I, for constant values of the quintessence parameter  $C$  and  $a = 0.1$ , the outer horizon  $r_+$  decreases as the charge  $Q$  increases, while for constant values of  $Q$  and  $a = 0.1$ , the outer radius increases as  $C$  increases.

On the other hand, according to Fig. 2, we found that the existence of the outer horizon  $r_+$  is constrained by the values of the charge  $Q$ . For example, in Fig. 2a (when  $Q = 0.03$ ), we see that  $r_+$  exists in the intervals:  $0 \leq a \leq 0.875$  ( $C = 0.01$ ),  $0 \leq a \leq 0.9$  ( $C = 0.02$ ),

and  $0 \leq a \leq 0.975$  ( $C = 0.03$ ) approximately. However, when  $Q = 0.09$  (see Fig. 2b),  $r_+$  exists in the intervals:  $0 \leq a \leq 0.775$ ,  $0 \leq a < 0.8$ , and  $0 \leq a < 0.825$  for  $C = 0.01$ ,  $C = 0.02$ , and  $C = 0.03$  respectively. In this sense, if we change the charge  $Q$  the outer horizon will be constrained to different intervals. Therefore, we conclude that  $r_+$  strongly depends on the charge  $Q$ , the spin parameter  $a$ , and the quintessence parameter  $C$ .

In the same way, we found that shape and size of the horizon and the ergosphere depend on the charge  $Q$ , the spin parameter  $a$ , and the quintessence parameter  $C$ . According to Fig. 4, when the spin parameter  $a$  is increased, we found that the radius of the event horizon decreases and the area of the ergo-region increases. A similar behaviour was observed when the charge  $Q$  was increased. In addition, by comparing Figs. 4a, b, and c with Figs. 4d, e, and f, we conclude that the increment of the ergo-region was greater when we increased the spin parameter  $a$ . On the other hand, we found that the ergosphere radius does depend on the charge  $Q$  at the equatorial plane (see Figs. 4 d, e and f) but does not depend on the spin parameter (see Figs.4a, b and c) when the spin parameter and the charge are keeping constant respectively. The last result agrees with that obtained in [24].

In section V, we studied the effective potential, and the specific energy and angular momentum of the co-rotating and counter-rotating circular orbits. We found that co-rotating test particles (those with  $E_+$ ) are able to move along circular orbits that are closer to the black hole having small energy when the spin parameter is increased (see Figs. 7a, b, and c). This is due to the dependence of  $r_+$  on the charge and the spin parameter as we have shown in Fig. 4.a, b, and c. On the other hand, we found that counter-rotating particles are allowed to move far from the horizon with greater specific energy than the co-rotating particles.

In this work we also found that the photon circular orbits do not depend strongly on the charge  $Q$ . The contribution in equation (70) due to the charge is small

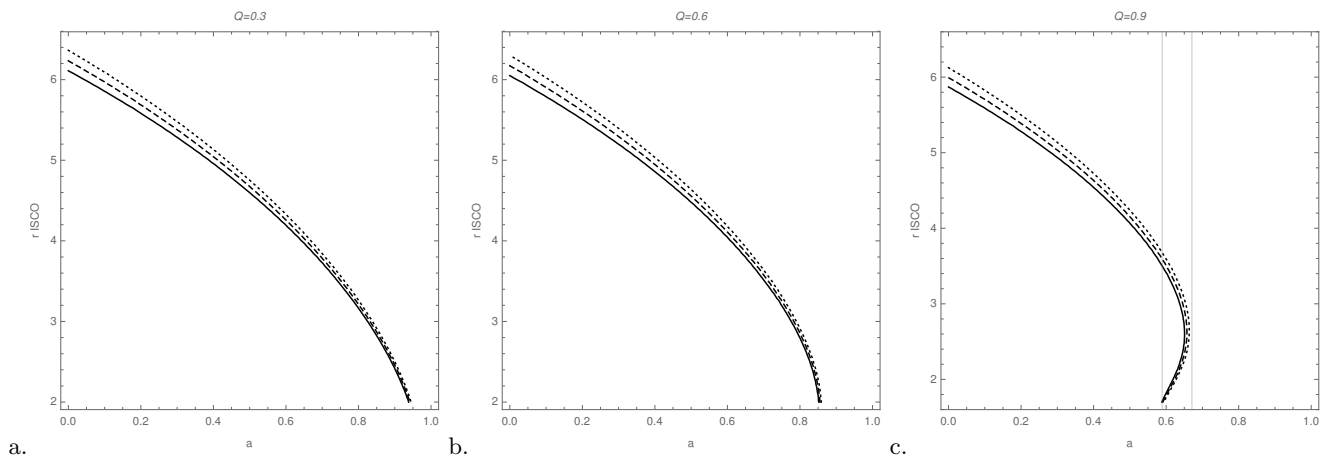


FIG. 9. Plot of  $r_{ISCO}$  vs.  $a$  for different values of  $Q$  when  $C = 0.001$  (Continuous line),  $C = 0.002$  (Dashed line),  $C = 0.003$  (Dotted line). In all the figures we considered  $M = 1$ , and  $\omega_q = -2/3$ .

even if we consider the interval  $0 \leq Q < 1$ . Therefore, equation (71) is in agreement with the limit imposed by the static radius  $r_C$ . This can be seen easily when comparing Tables II and III for  $C = 0.003$ .

Finally, we found that the innermost stable circular orbits are constrained to the values of the charge  $Q$ . For example, for  $Q = 0.03$ , Fig. 9 shows that  $r_{ISCO}$  exists only for values of  $a$  less than 0.95. When  $Q = 0.9$ , we see that  $r_{ISCO}$  exists for values of the spin parameter less than 0.7. Moreover, the  $r_{ISCO}$  increases as the value of the quintessence parameter  $C$  increases keeping the constrain (approximately) with the spin parameter  $a$ .

## ACKNOWLEDGMENTS

The authors thank Dmitry Ayzenberg, Askar Abdikalov and Pritom Mondal for helpful suggestions. This

work was supported by the National Natural Science Foundation of China (Grant No. U1531117) and Fudan University (Grant No. IDH1512060). C.A.B.G. also acknowledges support from the China Scholarship Council (CSC), grant No. 2017GXZ019022. The research is supported in part by Grant No. VA-FA-F-2-008 and No.YFA-Ftech-2018-8 of the Uzbekistan Ministry for Innovation Development, by the Abdus Salam International Centre for Theoretical Physics through Grant No. OEA-NT-01 and by Erasmus+ exchange grant between Silesian University in Opava and National University of Uzbekistan. A.A. thanks the Nazarbayev University for the hospitality.

- 
- [1] C. Bambi and A. D. Dolgov, *Introduction to Particle Cosmology: The Standard Model of Cosmology and its Open Problems* (Springer-Verlag, Berlin Heidelberg, 2016).
  - [2] S. Dodelson, *Modern Cosmology* (Academic Press, 2003).
  - [3] Planck Collaboration, P. A. R. Ade, N. Aghanim, C. Armitage-Caplan, M. Arnaud, M. Ashdown, F. Atri-Barandela, J. Aumont, C. Baccigalupi, A. J. Banday, and et al., *Astronomy and Astrophysics* **571**, A16 (2014), [arXiv:1303.5076](#).
  - [4] D. Kazanas, *Astrophys. J. Lett.* **241**, L59 (1980).
  - [5] A. A. Starobinsky, *Physics Letters B* **91**, 99 (1980).
  - [6] A. H. Guth, *Phys. Rev. D* **23**, 347 (1981).
  - [7] A. H. Guth and S.-Y. Pi, *Physical Review Letters* **49**, 1110 (1982).
  - [8] A. D. Linde, *Physics Letters B* **108**, 389 (1982).
  - [9] A. Albrecht and P. J. Steinhardt, *Physical Review Letters* **48**, 1220 (1982).
  - [10] A. G. Riess, A. V. Filippenko, P. Challis, A. Clocchiatti, A. Diercks, P. M. Garnavich, R. L. Gilliland, C. J. Hogan, S. Jha, R. P. Kirshner, B. Leibundgut, M. M. Phillips, D. Reiss, B. P. Schmidt, R. A. Schommer, R. C. Smith, J. Spyromilio, C. Stubbs, N. B. Suntzeff, and J. Tonry, *Astrophys. J.* **116**, 1009 (1998), [astro-ph/9805201](#).
  - [11] S. Perlmutter and et al., *Astrophys. J.* **517**, 565 (1999), [astro-ph/9812133](#).
  - [12] W. Yang, M. Shahalam, B. Pal, S. Pan, and A. Wang, ArXiv e-prints (2018), [arXiv:1810.08586 \[gr-qc\]](#).
  - [13] L. M. Krauss and M. S. Turner, *General Relativity and Gravitation* **27**, 1137 (1995), [astro-ph/9504003](#).
  - [14] S. Weinberg, *Reviews of Modern Physics* **61**, 1 (1989).
  - [15] P. J. Peebles and B. Ratra, *Reviews of Modern Physics* **75**, 559 (2003), [astro-ph/0207347](#).
  - [16] T. Padmanabhan, *Physics Reports* **380**, 235 (2003), [hep-th/0212290](#).

- [17] H. K. Jassal, J. S. Bagla, and T. Padmanabhan, *Phys. Rev. D* **72**, 103503 (2005), [astro-ph/0506748](#).
- [18] H. K. Jassal, J. S. Bagla, and T. Padmanabhan, *Mon. Not. R. Astron. Soc* **356**, L11 (2005), [astro-ph/0404378](#).
- [19] L. Samushia and B. Ratra, *Astrophys. J. Letter* **650**, L5 (2006), [astro-ph/0607301](#).
- [20] J.-Q. Xia, H. Li, G.-B. Zhao, and X. Zhang, *Phys. Rev. D* **78**, 083524 (2008), [arXiv:0807.3878](#).
- [21] X.-M. Z. B. F. G.-B. Zhao, J.-Q. Xia, *Int. J. Mod. Phys. D* **16**, 1229 (2007).
- [22] J.-Q. Xia, G.-B. Zhao, B. Feng, H. Li, and X. Zhang, *Phys. Rev. D* **73**, 063521 (2006), [astro-ph/0511625](#).
- [23] V. V. Kiselev, *ArXiv General Relativity and Quantum Cosmology e-prints* (2003), [gr-qc/0303031](#).
- [24] B. Toshmatov, Z. Stuchlík, and B. Ahmedov, *European Physical Journal Plus* **132**, 98 (2017).
- [25] V. V. Kiselev, *Classical and Quantum Gravity* **20**, 1187 (2003), [gr-qc/0210040](#).
- [26] S. Fernando, S. Meadows, and K. Reis, *International Journal of Theoretical Physics* **54**, 3634 (2015), [arXiv:1411.3192 \[gr-qc\]](#).
- [27] T. Oteev, A. Abdujabbarov, Z. Stuchlík, and B. Ahmedov, *Astrophys. Space Sci.* **361**, 269 (2016).
- [28] A. Abdujabbarov, B. Toshmatov, Z. Stuchlík, and B. Ahmedov, *International Journal of Modern Physics D* **26**, 1750051-239 (2017).
- [29] E. T. Newman and A. I. Janis, *Journal of Mathematical Physics* **6**, 915 (1965).
- [30] M. Broccoli and A. Viganò, *Phys. Rev. D* **98**, 084007 (2018), [arXiv:1807.08313 \[gr-qc\]](#).
- [31] H. Erbin, *Universe* **3**, 19 (2017), [arXiv:1701.00037 \[gr-qc\]](#).
- [32] E. J. Gonzalez de Urreta and M. Socolovsky, *ArXiv e-prints* (2015), [arXiv:1504.01728 \[gr-qc\]](#).
- [33] H. Erbin and L. Heurtier, *Classical and Quantum Gravity* **32**, 165004 (2015), [arXiv:1411.2030 \[gr-qc\]](#).
- [34] A. J. Keane, *Classical and Quantum Gravity* **31**, 155003 (2014), [arXiv:1407.4478 \[gr-qc\]](#).
- [35] C. Bambi and L. Modesto, *Physics Letters B* **721**, 329 (2013), [arXiv:1302.6075 \[gr-qc\]](#).
- [36] D. J. C. Lombardo, *Classical and Quantum Gravity* **21**, 1407 (2004).
- [37] M. Azreg-Aïnou, *Phys. Rev. D* **90**, 064041 (2014), [arXiv:1405.2569 \[gr-qc\]](#).
- [38] M. Azreg-Aïnou, *European Physical Journal C* **74**, 2865 (2014), [arXiv:1401.4292 \[gr-qc\]](#).
- [39] M. Azreg-Aïnou, *Classical and Quantum Gravity* **28**, 148001 (2011), [arXiv:1106.0970 \[gr-qc\]](#).
- [40] B. Toshmatov, B. Ahmedov, A. Abdujabbarov, and Z. Stuchlík, *Phys. Rev. D.* **89**, 104017 (2014), [arXiv:1404.6443 \[gr-qc\]](#).
- [41] C. H. Nam, *General Relativity and Gravitation* **50**, 57 (2018).
- [42] S. A. Hayward, *Physical Review Letters* **96**, 031103 (2006), [gr-qc/0506126](#).
- [43] C. Bambi, *Black Holes: A Laboratory for Testing Strong Gravity* (Springer, Singapore, 2017).
- [44] S. Carroll, *Spacetime and Geometry: An Introduction to General Relativity* (Benjamin Cummings, 2003).